# Dynamic SPECT Imaging Using a Single Camera Rotation (dSPECT) [1]

T. Farncombe[†], A. Celler[‡] *Member, IEEE*, D. Noll[¶], J. Maeght[¶], R. Harrop[‡] *Member, IEEE*
[†]Physics Department, University of British Columbia, Vancouver, B.C., Canada
[‡]Div. of Nuclear Medicine, Vancouver Hospital and Health Sciences Centre, Vancouver, B.C., Canada
[¶]Laboratoire Mathématiques pour l'Industrie et la Physique, Université Paul Sabatier, Toulouse, France.

## *Abstract*

Techniques to estimate dynamic parameters from the data acquired during a single rotation of a standard (single, dual and triple head) SPECT camera are being investigated. The performance of the constrained linear least squares (C-LS) method is being assessed. This method uses a simple assumption that the activity within each pixel at a given projection angle is less than or equal to the activity seen at the prior angle. In simulations, we have used an analytical heart model with single and bi-exponential activity decrease, with and without background activity and statistical noise in the data. Studies using a single, a 90° dual and a 120° triple head camera were modeled with a total acquisition time of 20min, performing rotation over 180°. These simulations were followed by experimental scans of our dynamic phantom used with and without attenuation and subsequently a preliminary study involving a human subject was performed. Dynamic images from simulations and phantom experiments reconstruct well with an accuracy of reconstructed half-lives for most reconstructions within a 20% error range. Some streaking artifacts which are evident in images corresponding to early reconstruction times subside upon incorporating further constraints and regularizations.

## I. Introduction

In conventional SPECT studies, radiopharmaceuticals which are injected into a patient are designed to be uptaken by an organ of interest and remain stationary in this organ throughout the acquisition time of the study. However, some radiopharmaceuticals (eg, Teboroxime, iodo-fatty acids, etc), after being uptaken by the organ are metabolized and/or washed out, thereby exhibiting biological half-lives on the order of minutes. It is thought that the rate of infusion and subsequent extraction of such pharmaceuticals from the tissue is a good indication of organ function [1]. The determination of these parameters is the subject of dynamic SPECT imaging.

Dynamic imaging in nuclear medicine is currently performed either with planar acquisition protocols, or in SPECT mode using multiple, fast rotations [2, 3]. Neither of these methods is ideal, however, as the planar method suffers from a lack of spatial resolution, and fast rotation SPECT requires special hardware and has poor image statistics.

Because of these concerns, we are investigating dynamic SPECT techniques which use only a single, slow camera rotation and can be implemented on any SPECT system (with one, two or three heads). We will refer to this class of methods as 'dSPECT'. In this paper we present a general outline of a new method for dSPECT data reconstruction, constrained linear least squares (C-LS), and discuss its results for simulated and experimental phantom data. Preliminary results from a dSPECT renal study of a human subject are also presented.

[1]We would like to acknowledge the support we have obtained for this project from the BC Health Research Foundation. Part of the travel expenses for one of us (T.F.) have been covered by the French Consulate in Vancouver.

## II. dSPECT Methods

We have been involved in the investigation of several different dSPECT reconstruction methods including a direct parameter reconstruction technique [4] which makes use of nonlinear least squares (NLS) to fit projection data and solve for kinetic parameters of an assumed dynamic model. Aside from taking a long time to perform a reconstruction, this method also makes assumptions as to the functional form of the dynamics involved which may or may not be correct. Other approaches which we investigated reconstructed series of dynamic images using nonlinear least squares [5] or a linear approach and EM-algorithm [6].

### *A. Constrained Linear Least Squares*

In this paper we present the results of reconstruction with the constrained linear least squares technique (C-LS). The C-LS method uses the entire data set to reconstruct a series of images representing the change in activity distribution over time. The advantage of this approach is that it makes no strict assumptions as to the functional behaviour of tracer over time but rather makes the minimal assumption that the activity within each voxel when measured at a given projection angle (ie. projection time) is less than, or equal to, the activity present in the same voxel at the previous projection angle. Thus we are solving a linear least squares problem of the form:

$$f(x) = \left\{ \sum_{j,k} \sigma_{jk}^{-2} \left( \sum_{i} a_{ijk} x_{ik} - d_{jk} \right)^2 \right\} \qquad (1)$$

subject to,

$$x_{i1} \geq x_{i2} \geq \ldots \geq x_{in} \geq 0 \qquad (2)$$

where $\sigma_{jk}^{-2}$ is a weighting factor determined from the variance of the projection bin contents $d_{jk}$; $a_{ijk}$ is a geometrical weighting factor that may or may not incorporate attenuation and collimator blurring; and $x_{ik}$ is the vector containing the

unknown activity distribution at the time the k-*th* projection is acquired.

In order to stabilize the problem, we may add various regularizing terms to the quadratic objective, for instance, Tychonoff type regularization or terms incorporating prior information regarding the expected reconstruction.

As mentioned before, with this technique, a series of images is reconstructed where each image corresponds to the activity distribution at the time when each projection is acquired. In the present implementation, each dynamic slice is reconstructed separately and the image of the whole 4D (3D+time) distribution is obtained by stacking these slices together. Analysis of kinetic parameters is then carried out where 2D or 3D regions of interest (ROI) are drawn on the images and copied to succeeding images with the counts obtained within each region plotted as a function of time.

Notice that for a typical image slice of size $64 \times 64$, reconstructed from data acquired over 64 projections, each containing 64 bins, the C-LS approach requires solving a quadratic problem with $64^3$ unknowns, a considerably larger dimension than that of the non-linear least squares which has $5 \cdot 64^2$ degrees of freedom in the case of dual exponential + constant fitting. Nevertheless, the advantage of the C-LS method is that it converges fast (10 – 20 minutes for a slice (64x64) versus 1 – 2 hours needed by NLS when performed on a Pentium II 400 MHz), and that the time needed to perform the *a posteriori* curve fitting is negligible.

A modified approach attempting to seek a compromise between NLS and C-LS, is currently under investigation. Using the fact that a dual exponential function may be replaced by a linear difference equation of the form:

$$x_{i,k+1} = \alpha_i x_{i,k} + \beta_i x_{i,k-1} + \gamma_i, \tag{3}$$

we propose to minimize:

$$\tilde{f}(x) = f(x) + F(x) + S(x) \tag{4}$$

where:

$$F(x) = K \sum_i \left( \sum_k x_{i,k+1} - \alpha_i x_{i,k} - \beta_i x_{i,k-1} - \gamma_i \right)^2 \tag{5}$$

Again $f(x)$ is the same as previously used in the C-LS method and $S(x)$ is some type of spatial regularization (eg. Tychonoff, Boltzmann-Shannon, etc). Again we minimize $\tilde{f}(x)$ subject to the constraint in (2).

Starting with $K = 0$ we first obtain an estimate for $x_{i,k}$. Based on $x_{i,k}$, we estimate the parameters $\alpha_i, \beta_i$ and $\gamma_i$ for each pixel $i$, which is the same as fitting a biexponential model to the calculated $x_{i,k}$. With $\alpha_i, \beta_i$ and $\gamma_i$ estimated, and with a choice of $K > 0$, we repeat the procedure to obtain an improved estimate of $x_i$. This may be repeated several times and, with increasing $K > 0$, may be seen to converge to a set of decay curves $x_{i,k}$ which (for each pixel) will be close to the respective biexponential decays. In practice, only a few steps should suffice with the proper choice of the penalty term $K$.

### B. *Incorporation of Attenuation Correction*

One of the primary concerns in dynamic SPECT is the problem of attenuation as changes in activity distribution detected in subsequent projections due to attenuation cannot be distinguished from changes due to dynamic processes. Attenuation correction is typically performed by adjusting the pixel weighting factors $a_{ijk}$ according to values obtained from attenuation maps. These attenuation maps can be determined from transmission scans acquired simultaneously with the dynamic emission studies [7].

Because the dynamic reconstruction is performed using only a very limited number of counts, special attention should be paid to the quantitative accuracy of attenuation correction since large uncertainties in these corrections may have a very detrimental effect on the quality of reconstruction. Several tests incorporating attenuation were performed using both the dynamic phantom and human subject in order to further investigate this issue.

## III. Simulations and Experiments

In our computer simulations we have used an analytical heart model in the shape of an annulus divided into four equal sections. This shape was designed to test the performance of the method in a difficult case where different dynamic behaviour is present in several regions of the same object and these data overlap in the projections. Each section was assumed to have the same activity concentration at the initial moment $t_0$ and was subsequently washed out at different rates. In our tests, we have modeled single and dual exponential washout, with and without background activity, and with and without statistical noise. Simulated washout times for four heart sections were 2min, 4min, 10min and static activity for the case of monoexponential washout, and 2min+10min, 4min+15min, 10min+20min and static for dual exponential washout. Noise-free data were generated and reconstructed to test the performance of the method under 'ideal' conditions. Additionally, background static activity equal to 5% of the initial heart activity was assumed in some simulations along with a random Poisson noise corresponding to the initial activity of 1.85MBq (0.05mCi) in each section. Projections were generated in 128x128 matrices and corresponded to acquisitions of 64 projections over total study times equal to 20min and involving camera rotations over 180° of single and triple head cameras, and over 90° for each head of the dual head system with heads at 90°. Reconstruction using the C-LS algorithm was investigated in all cases.

Phantom experiments were performed using a dynamic heart model which is a part of our dynamic heart-in-thorax phantom [8]. The initial activity levels ranged from 18MBq (0.5mCi) up to 75MBq (2mCi) in each container. In all phantom experiments the activity washout followed a mono-exponential function.

In the first series of phantom experiments, four bottles of equal size (17ml) with washout times ranging from 2.7min to 7.0min were positioned asymmetrically on the camera bed with no additional attenuating material. A Siemens triple head MS3 camera was used with 64 projections per head acquired into a 64x64 matrix. Acquisition time for each projection was set to be 10 seconds which resulted in a total acquisition time of about 12min. Data from all three heads was collected concurrently with each head rotating over 180°. Reconstructions were performed using data from all three heads simultaneously (triple head acquisition) and using one head only (single head acquisition).

The second series of experiments was designed to test the attenuation effect. In this case the phantom contained three small bottles of equal size (17 ml) positioned symmetrically around a larger (32ml) volume containing static activity. The washout times in the three small containers were 2min, 3min and 6min. To model the effect of attenuation, these four bottles were submerged in a larger (500ml) water volume not containing activity with two additional cold water bags (8 liters total volume) placed on top of the phantom. Data was collected using a Siemens Ecam dual head SPECT camera with the heads positioned at 90°. Attenuation maps were obtained from transmission data acquired simultaneously with the dynamic emission study using a multiple line source *Profile* system [9]. The acquisition protocol consisted of a single camera rotation with each head moving over 90° (total rotation of 180° for two heads) for a 12 min total duration of the scan. A total of 128 projections (2 x 64) of size 128x128 were acquired with each projection taking 10 seconds.

As an additional test of the performance of the reconstruction method and to check the images for the possible overlap of the reconstructed activity originating from different containers, each bottle was imaged separately (data set A) and, at the end, the projection data for all containers were summed together to create a sinogram consisting of all objects (data set B). By using this method, we were able to reconstruct and analyze the data from each single container separately to confirm the dynamic behaviour of washout of the activity and to compare the quality of these single object reconstructions with those where all containers were reconstructed at the same time. We were also able to assess more accurately the exact effect of attenuation on our acquisition data. At the end of each experiment, a simultaneous acquisition of all bottles was performed (data set C) to further verify the consistency of our approach.

In the initial patient study, the injection of 370MBq of $^{99m}$Tc MAG3 was used with an acquisition protocol consisting of sequential 180° and −180° rotations, again with the Siemens Ecam camera with the heads in the 90° configuration. In order to provide attenuation correction, dynamic emission data was again collected simultaneously with the transmission data as in the phantom experiment. Between rotations, the data had to be saved, which resulted in a 2.5 minute pause in the data collection process. The total time of each acquisition was equal to 12 minutes and a total of 128 projections per rotation, with a 128x128 matrix size were collected. The data from the first rotation contained information related to the washin and the washout of the activity, while the second part of each study imaged only the decrease of activity. In this paper, only reconstruction of the data from the second scan containing the washout part the study is discussed.

In order to validate the performance of the dSPECT reconstruction, a dynamic planar study was performed several hours prior to the dSPECT scan. This scan consisted of the injection of 55 MBq of $MAG3$ followed by dynamic planar imaging using a Siemens Diacam single head camera. Planar data was collected in 5 second frames for a total scan time of 25 minutes and then rebinned into 10 second frames so as to correspond to the same time interval as in the subsequent SPECT scan.

## IV. Data Analysis

In order to assess the accuracy of our reconstructions we have analyzed a figure of merit ($\mathcal{M}$) score which compares the 'true' number of counts as assumed to be in the voxels of the object with the reconstructed values. Since reconstructions are performed one slice at a time, $\mathcal{M}$ was calculated separately for each slice. Extension of the method into 3D is straightforward. As the true counts are only known for simulated data, $\mathcal{M}$ values are only reported for these cases.

As our method reconstructs a series of images, the number of counts in each reconstructed image corresponds to the total number of photons detected by the camera over the time the projection is acquired. In order to compare the 'true' counts in the object with the reconstructed counts, we have estimated the 'true' number of counts, $x_{ik}$ in each i-*th* object voxel integrated over the acquisition time for a given k-*th* projection and compared it with the corresponding reconstructed value $\tilde{x}_{i,k}$. This procedure has been repeated for each time frame k. To minimize the effect of statistical fluctuations, the sum over an ROI containing N voxels normalized by the total 'true' counts in this ROI was used. This sum was calculated over all voxels for each of the heart sections.

$$\mathcal{M}_{ROI} = \sqrt{\frac{\sum_{i=1}^{N}(x_{i,k} - \tilde{x}_{i,k})^2}{\sum_i x_{i,k}^2}} \tag{6}$$

Plotting the values of $\mathcal{M}_{ROI}$ for each k-*th* time frame versus the frame number provides us with information as to how the method performs at different stages of the dynamic process. Summing the M values for all time frames and normalizing for the acquisition time of each frame provides an overall estimate as to the quality of reconstruction for a given ROI. Calculating $\mathcal{M}_{ROI}$ over regions with different dynamic behaviour allows for comparison of the performance of the method under different conditions. For example, by comparing $\mathcal{M}_{ROI}$ for regions with fast dynamic washout and those with slow washout, we are able to assess the accuracy of reconstruction for different total acquisition times. Similar sums calculated over all the voxels of the whole image space ($\mathcal{M}_{tot}$) provides an indication of the overall performance

of the reconstruction. Investigation of these values allows for objective comparison of the quality of reconstruction for different sets of parameters, noise levels, iteration stopping criteria, etc.

In parallel, in order to determine accuracy of the reconstructed values of the washout half-life, analysis was carried out for each ROI of the reconstructed series of dynamic 2D images by plotting counts vs time, and then fitting this data with an appropriate mono or dual-exponential function. For the experimental phantom data, a sum over 3x3 voxel ROI's placed at the center of each object of the phantom was used. For simulations the summation was performed over all pixels in each dynamic ROI. This value was then compared to the actual washout half-life preset in the simulation or in the experiment. Similarly, the initial number of counts $N_0$ as assumed in the object ('true values') was compared with those obtained from the reconstructed images. For the patient data the 'truth' was not known and therefore only a comparison of the dSPECT results with the data obtained in the planar scan (not corrected for attenuation) was possible.

## V. Results

### A. Simulated Data

C-LS results from simulated data acquired with a 180° rotation of a single head camera are depicted in Figure 1. Reconstructions were performed with constraint (2) and with constraint (5) for data consisting of monoexponential washout for both noiseless projection data and with Poisson noise added.

As can be seen from this figure, the reconstructed images clearly display the effect of different washout rates for each heart section. The agreement between the reconstructed half-lives and the preset values is about 10% in this case and improves upon using lower stopping criteria in the reconstruction procedure. Reconstructions from noisy data have errors very comparable to the noiseless case. Some C-LS reconstructions show artifacts which can be removed by *a posteriori* filtering or by using spatial restrictions. The case of single head acquisition certainly represents the most difficult situation. Much improved images have been obtained when reconstructing data from simulations involving dual or triple head cameras.

An example of the analysis of the accuracy of the reconstructions for the data shown on Figure 1 is presented in Table 1. Results obtained in reconstructions using the modified approach of (5) demonstrate better agreement with the true values than those obtained in unrestricted reconstructions. These results are still preliminary and we believe that further optimization of the reconstruction parameters will dramatically improve the accuracy of reconstruction.

### B. Experimental Data

As mentioned, experiments have been performed using our dynamic heart phantom in a variety of configurations and

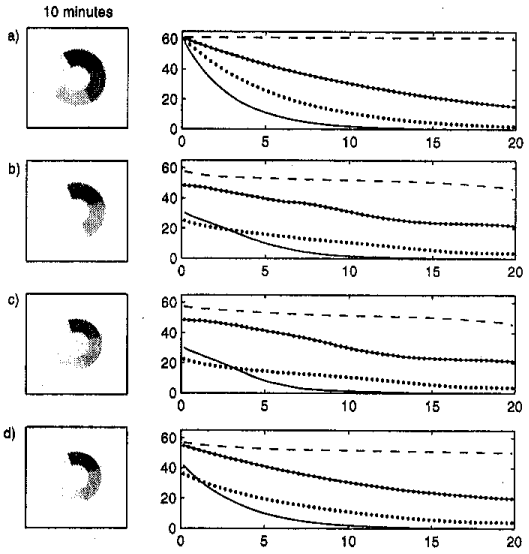


Figure 1: C-LS reconstructions of simulated data acquired with a single 180° rotation of a single head camera. (a) True image at t=10 minutes along with time activity curves used in simulations ('the truth'). (b) Image and the time-activity curves obtained from the reconstruction using only the constraint (2) with noiseless data. (c) Image and time-activity curves from the data containing Poisson noise and background activity reconstructed with (2). (d) Image and time-activity curves from the data containing Poisson noise and background activity reconstructed with (5).

| | True $T_{1/2}$ (min) | Recon $T_{1/2}$ (min) | True $N_0$ | Recon $N_0$ | $\mathcal{M}_{ROI}$ | $\mathcal{M}_{tot}$ |
|---|---|---|---|---|---|---|
| with (2) | 2 | 1.9 | 58 | 39.8 | 0.429 | |
| | 4 | 6.8 | 58 | 22.3 | 0.604 | |
| | 10 | 12.2 | 58 | 51.0 | 0.288 | |
| | static | 93 | 58 | 61.8 | 0.204 | |
| | | | | | | 0.329 |
| with (5) | 2 | 1.9 | 58 | 52.5 | 0.364 | |
| | 4 | 5.2 | 58 | 34.8 | 0.428 | |
| | 10 | 11.1 | 58 | 54.3 | 0.291 | |
| | static | 201 | 58 | 59.9 | 0.200 | |
| | | | | | | 0.285 |

Table 1: Analysis of the accuracy of C-LS reconstructions of the dynamic analytical heart simulations. The data have been generated with a single 180° rotation of a single camera head (see text for details).

with various washout parameters. The data from experiments performed using only one dynamic bottle at a time (data set A) were used to confirm the time-calibration ('true $T_{1/2}$') of our phantom and to provide information about the initial activity in the bottle ('true $N_0$'). The procedure was as follows: the values of the washout half-life preset for each container (phantom time calibration) were verified by fitting an exponential function to the total projection data for each bottle (data set

A), similarly the total number of counts in the first projection provided information regarding the initial activity in the bottle. Next, the projection data from all experiments were summed together (forming data set B) and reconstructed. The results of these reconstructions were almost identical to the images obtained from simultaneous acquisitions of all bottles together (data set C) and also compared quite well with the results of single bottle acquisitions (data set A). All images presented in this paper were obtained using data set B.

Tests performed using a Siemens MS3 triple head camera without attenuation were employed to compare the quality of reconstructions from the data acquired with one head only with the data from all three heads. Reconstructions were obtained using the C-LS method for the case of single and triple head acquisitions. Figures 2 and 3 display the results of these reconstructions (with constraint (2)) for the single and the triple head acquisition, respectively. As can be seen in these images stronger streaking artifacts are present in the single head rotation than in the triple head images.

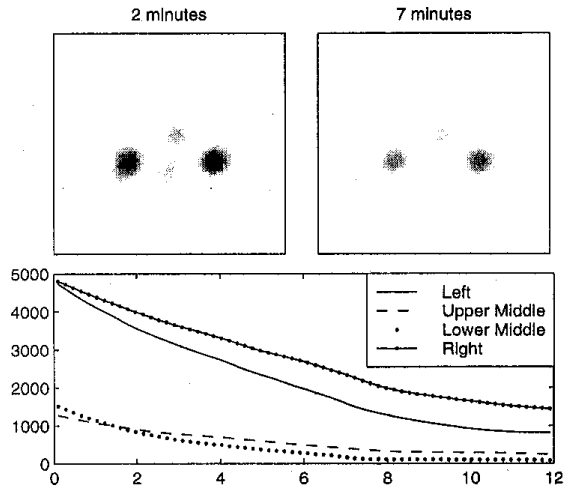


Figure 2: Dynamic images obtained using C-LS reconstruction with (2) performed with data acquired with a single head of a MS3 triple head camera (upper) and the time activity curves for each container (lower).

The analysis of the accuracy of the reconstructed values of the washout half-life was performed using the same method as in simulation studies, except that the 'true' value of the washout half-life of each phantom element was found from the single bottle acquisitions. Table 2 presents the results of these studies. The agreement between the values determined from single bottle and full phantom acquisitions in the case of triple camera scans was better than for single camera acquisition. This result is easy to understand as a triple head camera contains three independent views of the spatial distribution at each time, whereas only a single view is obtained at a time with a single head camera. As with the results obtained for simulated data, reconstructions using (5) demonstrate much better agreement with the true values than those obtained in unrestricted reconstructions.

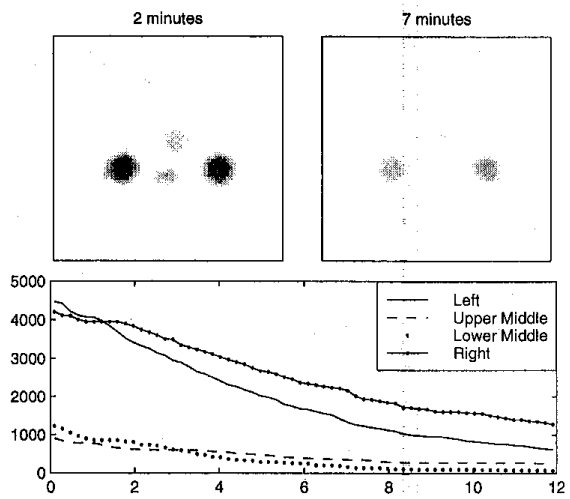


Figure 3: Dynamic images obtained using C-LS reconstruction with (2) performed using the data acquired with all three head of a triple head MS3 camera (upper) and the time activity curves for each container (lower).

| | True $T_{1/2}$ (min) | Recon $T_{1/2}$ (min) | True $N_0$ (cnts) | Recon $N_0$ (cnts) | % Diff in $T_{1/2}$ |
|---|---|---|---|---|---|
| 1 head acquisition with (2) | 7.0 | 6.2 | 1830 | 1510 | 11 % |
| | 6.7 | 5.4 | 5532 | 4807 | 19 % |
| | 2.7 | 4.3 | 1705 | 1288 | 60 % |
| | 3.8 | 4.0 | 6167 | 4593 | 5 % |
| 1 head acquisition with (5) | 7.0 | 6.8 | 1830 | 1665 | 2 % |
| | 6.7 | 5.1 | 5532 | 4730 | 23 % |
| | 2.7 | 3.5 | 1705 | 1476 | 31 % |
| | 3.8 | 4.6 | 6167 | 4960 | 21 % |
| 3 head acquisition with (2) | 7.0 | 7.0 | 1830 | 980 | 1 % |
| | 6.7 | 6.9 | 5532 | 4233 | 3 % |
| | 2.7 | 2.9 | 1705 | 1198 | 7 % |
| | 3.8 | 4.2 | 6167 | 4570 | 12 % |

Table 2: Analysis of the accuracy of C-LS reconstructions of the dynamic phantom experiments performed using MS3 triple head camera (for details see text).

The second series of phantom experiments included attenuation and was performed using a dual head Ecam camera with heads at $90^o$ as this camera has hardware which allows for the acquisition of patient specific attenuation maps. Figure 4 displays a typical reconstruction using the modified approach (5) from such an experiment along with the reconstructed time-activity curves for all four dynamic containers. The analysis of the accuracy of the half-lives obtained from these reconstructions is presented in Table 3. Because of attenuation no 'true' $N_0$ was available for these experiments. The results of these reconstructions when compared to those obtained without attenuation clearly demonstrate that our method performs well even in this difficult case and that dynamic images can be successfully reconstructed for situations involving attenuation.

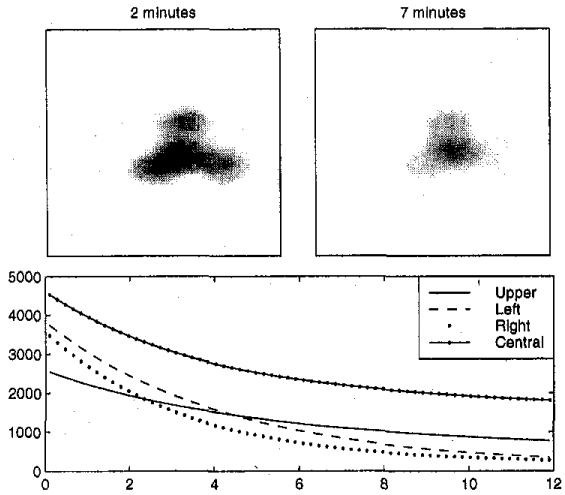


Figure 4: Dynamic images obtained from C-LS reconstruction of the phantom data with attenuation (upper) and the resultant time activity curves for each dynamic container (lower).

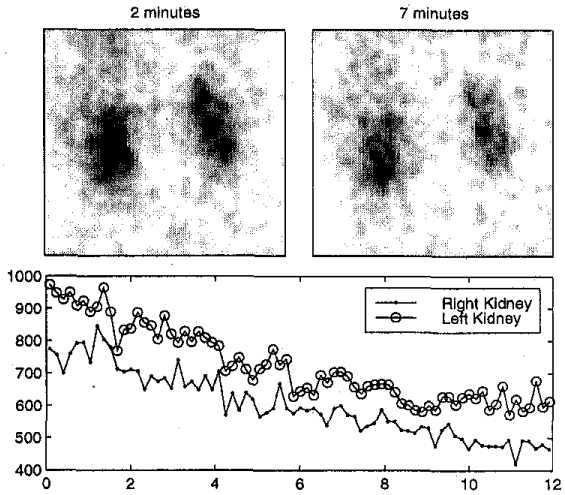


Figure 5: Planar images of a patient MAG3 scan acquired for 12min over the second, 13-25min, period with an acquisition of 5 seconds per frame (upper). The resultant time activity curves for each kidney (lower).

| | Ideal $T_{1/2}$ (min) | Recon $T_{1/2}$ (min) | % Difference in $T_{1/2}$ |
|---|---|---|---|
| 2 head | 2 | 2.73 | 37% |
| acquisition | 3 | 3.47 | 16% |
| with | 6 | 6.63 | 11% |
| (5) | static | 9.27 | N/A |

Table 3: Analysis of the accuracy of C-LS reconstructions of the dynamic phantom experiments performed using Ecam dual head camera with attenuation correction(for details see text).

Patient scans correspond to situations much more complex than any phantom experiment and so we have investigated the performance of the C-LS reconstruction using data acquired with a human subject. The experimental conditions using the second part of the patient studies were quite similar to those used in the last series of phantom experiments (with attenuation). The second rotation of the patient acquisition was performed at the time 13-25min post injection as by this time the activity uptake was no longer visible and only the washout of the activity was observed. Since in this case the true washout half-lives were unknown, the values obtained from the C-LS reconstruction were compared with those obtained from planar dynamic studies. Figure 5 shows two images from the planar scan while Figure 6 shows similar images obtained by the reprojection of 24 slices reconstructed from the dSPECT data. In both cases the time activity curves for each kidney are also presented. These reconstructions were performed without restrictions (constraint 2) because it was not known *a priori* if the functional dependence of the activity washout is bi-exponential. As can be seen from Table 4, when the $T_{1/2}$ values obtained in these two studies are compared, their agreement is 15% and 10% for the left and right kidney, respectively. Figure 7 presents one transaxial slice from the dSPECT images used in the creation of Figure 6.

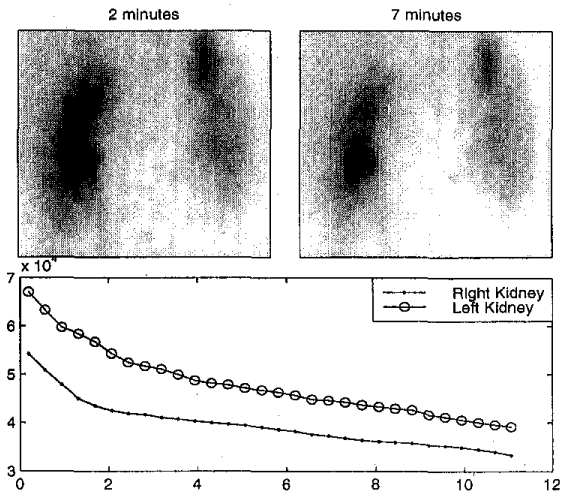


Figure 6: Planar images obtained from the reprojection of 25 reconstructed slices of the dSPECT images of a patient MAG3 scan acquired for 12min over the second, 13-25min, period with an acquisition of 10 seconds per frame (upper). The resultant time activity curve for each kidney (lower).

| | Planar $T_{1/2}$ (min) | Recon $T_{1/2}$ (min) | % Diffeerence |
|---|---|---|---|
| Left Kidney | 16.2 | 18.6 | 15% |
| Right Kidney | 17.7 | 15.9 | 10% |

Table 4: Values of the washout half-lives from the second part of the patient study. The scans were performed using Ecam dual head camera with attenuation correction and reconstructions used C-LS method without (5.)

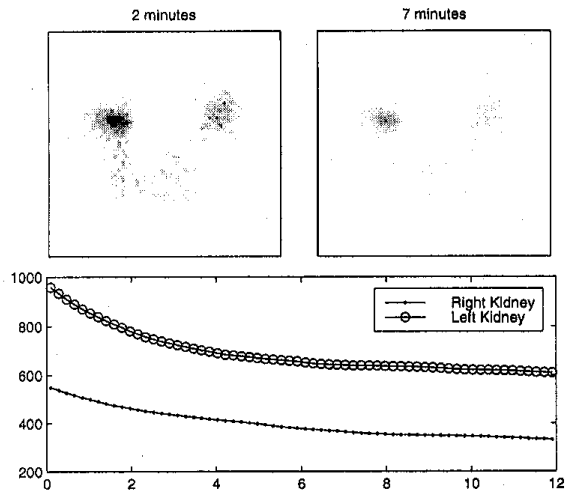


Figure 7: A single slice of the dSPECT images of a patient MAG3 scan acquired over the 13-25 minute period with an acquisition of 10 seconds per frame (upper). The time activity curves for each kidney obtained from this slice (lower).

### C. Conclusions

In this work, a new method of estimating kinetic parameters from dynamic SPECT data was investigated. A particularly important advantage of this method is that it allows estimation of the kinetic parameters of the dynamic processes in the scanned object when using only a single camera rotation and acquisition protocols similar to those used in standard SPECT studies.

Several simulation and phantom experiments were performed using single and dual exponential washout functions with different acquisition protocols and camera geometries. In some scans, attenuation effects were included and the subsequent reconstructions performed with attenuation correction.

The reconstruction using the C-LS method is much faster than nonlinear least squares methods with comparable accuracy of results, but with much more flexibility. Although the images obtained from dSPECT acquisitions using our reconstruction method provide satisfactory images with proper spatial distributions, the errors of the reconstructed half-lives still remain too high. In order to improve the accuracy of reconstruction, intensive studies of the acquisition protocols and parameters used in calculations are being conducted. We are optimistic that once the acquisition procedure is optimized, these results will improve significantly.

## VI. References

[1] S. Nellis, A. Liedtke, and B. Renstrom, "Fatty acid kinetics in aerobic myocardium:Characteristics of tracer carbon entry and washout and influence of metabolic demand," *J. Nuc. Med.*, vol. 33, pp. 1864–1874, 1992.

[2] A. Smith and G. Gullberg, "Dynamic cardiac SPECT computer simulations for teboroxime kinetics," *IEEE Trans. Nuc. Sci.*, vol. 41, pp. 1626–1633, 1994.

[3] K. Nakajima, N. Shuke, J. Taki, T. Ichihara, N. Motomura, H. Bunko, and K. Hisada, "A simulation of dynamic SPECT using radiopharmaceuticals with rapid clearance," *J. Nuc. Med.*, vol. 33, pp. 1200–1206, 1992.

[4] M. Limber, A. Celler, J. Barney, M. Limber, and J. Borwein, "Direct reconstruction of functional parameters for dynamic SPECT," *IEEE Trans. Nuc. Sci.*, vol. 42, pp. 1249–1256, 1995.

[5] E. Hebber, D. Oldenburg, T. Farncombe, and A. Celler, "Direct estimation of dynamic parameters in SPECT tomography," *IEEE Trans. Nuc. Sci.*, vol. 44, no. 6, pp. 2425–2430, 1997.

[6] H. Bauschke, D. Noll, A. Celler, and J. Borwein, "An EM-algorithm for dynamic SPECT tomography," *IEEE Trans. Med. Img.*, 1997. Submitted [CECM research report 97-092].

[7] A. Celler, T. Farncombe, D. Noll, J. Maeght, and R. Harrop, "Three approaches to dynamic SPECT imaging," in *1997 IEEE Nuclear Science Symposium Conference Record*, November 1997.

[8] A. Celler, A. Sitek, E. Stoub, D. Lyster, C. Dykstra, D. Worsley, and A. Fung, "Development of a multiple line source attenuation array for SPECT transmission scans," *J. Nucl. Med.*, vol. 38, no. 5, p. 215P, 1997.

[9] A. Celler, A. Sitek, E. Stoub, P. Hawman, R. Harrop, and D. Lyster, "Investigation of an array of multiple line sources for SPECT transmission scans: Simulation, phantom and patient studies," *J. Nuc. Med.*, vol. 39, no. 12, 1998.